

# An Experimental and Numerical Investigation on Vulcanized Fiber

Kardelen Bayram, Marcus Pfeiffer, Christian Alter, Stefan Kolling

Institute of Mechanics and Materials  
Technische Hochschule Mittelhessen, Giessen, Germany

## Abstract

As the automotive industry and its companies start to look for sustainability, materials made of natural fibers receive a growing interest. In the present work, the mechanical properties of a vulcanized fiber material were investigated to understand the orthotropic and rate-dependent material behavior and make it more predictable and thus practicable. **\*MAT\_PAPER** was used to represent the anisotropic elastic-plastic behavior of the material for crash and impact simulations.

To confirm numerical results from explicit FEM calculations, a user material subroutine comparable to **\*MAT\_PAPER** was utilized. Therefore, it was possible to perform implicit calculations of the conducted validation experiments which were performed at low strain rates.

## 1 Introduction

Although vulcanized fiber was discovered and patented over one hundred years ago [1], its full potential in engineering applications has not been exploited yet. Back then, vulcanized fiber replaced deep dawning products made of rubber and leather e.g. suitcases [2] due to its similar properties and appearance. It provides electrical insulating properties and was used in e.g. circuit breakers [3]. In many applications it was displaced by fully synthetic plastics. Currently, vulcanized fiber is used as carrier material for grinding discs due to its strength but light weight ratio. Other applications are, e.g. gaskets and washers [2].

Vulcanized fiber is a laminated plastic made by vulcanization of paper plies consisting of pure cellulose [1, 3]. During the process, cellulose plies pass through a bath containing either heated zinc chloride or low temperature sulfuric acid, which both work as a catalyst [4]. In case of the tested material Dynal<sup>®</sup> vulcanized fiber, provided by DYNOS<sup>®</sup>, a zinc chloride solution is used. This makes the paper plies' surfaces gelatinous [5]. The catalyst ensures the joining of the individual layers with one another, so no additional glue or binder is needed. Then, the zinc chloride is washed out and the product is dried, and calender rolled. The final product usually decomposes completely [6], unlike e.g. bioplastics. As a cost-effective and eco-friendly material it promises sustainability in technical advancement.

Besides polymer-like mechanical properties, such as comparably high yield strength and strain to failure [4], further important properties are the insensitivity to oils, greases, and organic solvents [2]. Additionally, its electrical insulation and flame retardancy allows for its use in a wide range of applications [3]. This makes it interesting for several modern applications in e.g. electric mobility.

To obtain the necessary material parameters, the vulcanized fiber material was tested for its anisotropic in-plane properties by cutting out specimens in different in-plane directions: MD (machine direction), CD (cross direction) and 45° (in between). The 45° off-axis tensile tests were used to determine the in-plane shear behavior. Before testing, the material specimens were preconditioned at 23° C and 50 % RH. A digital image correlation (DIC) system was used to determine the strain field during tensile tests. From the resulting stress-strain curves for a specific test speed the elastic and plastic parameters were evaluated, according to the material card **\*MAT\_PAPER**. Additionally, punch tests were performed to validate the material card for multiaxial loading situations.

**\*MAT\_PAPER** is an orthotropic elastoplastic material model to represent the behavior of paperboard. It is implemented for explicit simulations only. For shell elements, a hypoelastic-plastic formulation is used [7].

The user material subroutine (UMAT) uses a slightly simplified version of the in-plane yield criterion used in **\*MAT\_PAPER** and originally presented in [8]

$$f = \alpha_1 \left( \frac{\sigma_1 - \xi_1 \sigma_2}{R_1} \right)^2 + \alpha_2 \left( \frac{\sigma_2 - \xi_2 \sigma_1}{R_2} \right)^2 + \alpha_3 \left( \frac{-\sigma_1}{R_{1,c}} \right)^2 + \alpha_4 \left( \frac{-\sigma_2}{R_{2,c}} \right)^2 + \alpha_5 \left( \frac{|\tau|}{R_\tau} \right)^2 - 1 \quad (1)$$

with individual hardening variables for the different sub-surfaces. In [10] the criterion was used together with a non-associated flow rule. In this work an associated flow rule

$$\dot{\epsilon}_p = \lambda \frac{\partial \sigma f}{\|\partial \sigma f\|} \quad (2)$$

is utilized [9] and the out-of-plane normal and shear behavior is assumed to be completely elastic.

## 2 Experimental investigation

To determine all material parameters used within **\*MAT\_PAPER**, different experimental setups are necessary, see e.g. [10]. In this work, a reduced experimental setup by performing tensile tests was utilized to determine the material parameters governing the in-plane behavior of Dynal<sup>®</sup>. Simplifications led to estimations of the other parameters to fully describe the material behavior.

### 2.1 Tensile tests

In order to obtain the material parameters for **\*MAT\_PAPER** tensile tests were performed under constant loading velocities of 5 mm/min and 500 mm/min which result in strain rates of ~0.001 /s and ~0.1 /s, respectively (see Fig. 3 a). The considered in-plane directions (MD, CD and 45°) were tested five times for both loading velocities to ensure repeatability. The specimens were cut out from 0.8 mm thick DIN A4 sheets to a width of 15 mm using a guillotine. The width was measured at three different positions and the mean value was used to determine the stress. Before testing, the specimens were preconditioned at 23° C and 50 % RH for at least 24 h to provide comparability by eliminating long term temperature and humidity effects. All tests were carried out under laboratory conditions in a range of 20-25° C and 31-32% RH.

The specimens were pneumatically clamped at a free span length of 75 mm and a 5 kN load cell was used. GOM Aramis 12M digital image correlation (DIC) system was used to obtain the strain field of the specimen. The engineering stress

$$\sigma_0 = \frac{F}{A_0} \quad (3)$$

was calculated from the measured force  $F$  divided by the initial cross-sectional area  $A_0$ . The Hencky strain was determined as a mean value over the whole specimen area using DIC, see Fig. 1.

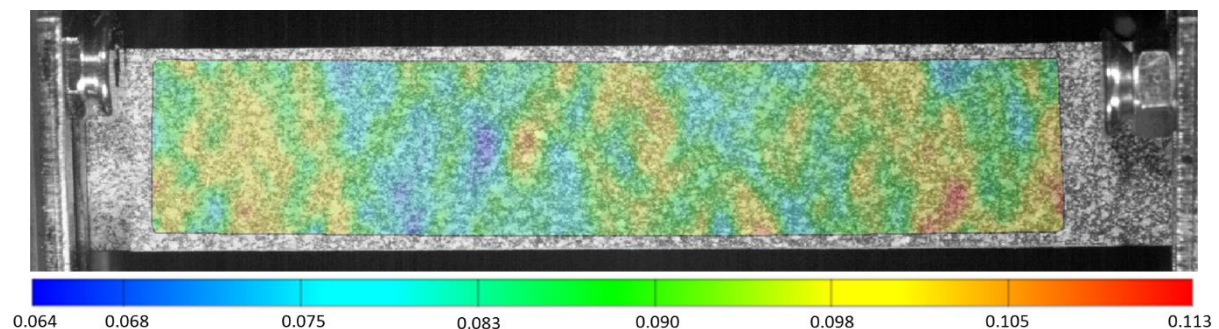


Fig. 1: Exemplary axial strain distribution from DIC measurement for uniaxial tensile test of Dynal<sup>®</sup>

Engineering stress vs. Hencky strain curves for the conducted tests for 5 mm/min and 500 mm/min are shown in Fig. 2a and 2b, respectively. An increased loading velocity results in higher stresses i.e. the material shows viscous behavior.

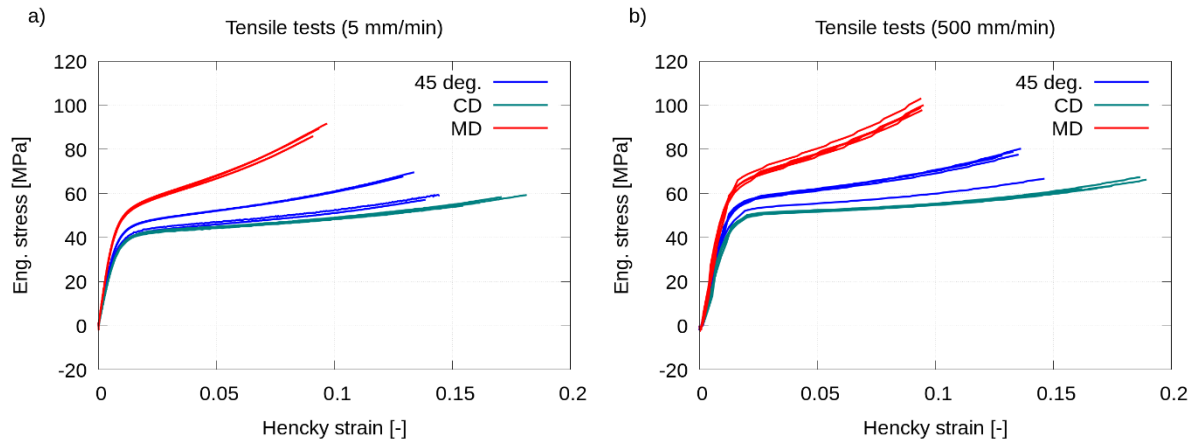


Fig.2: Eng. stress vs. Hencky strain for three in-plane directions (MD, CD, 45°) for a) 5 mm/min and b) 500 mm/min

Figure 3 a) exemplary shows the strain rates for all experiments in CD. The strain rate was calculated via the strain increments derived from DIC with respect to the frame rate divided by the corresponding time step. Figure 3 b) shows the lateral vs. axial Hencky strain obtained from DIC measurements in MD, CD and 45° at 5 mm/min.

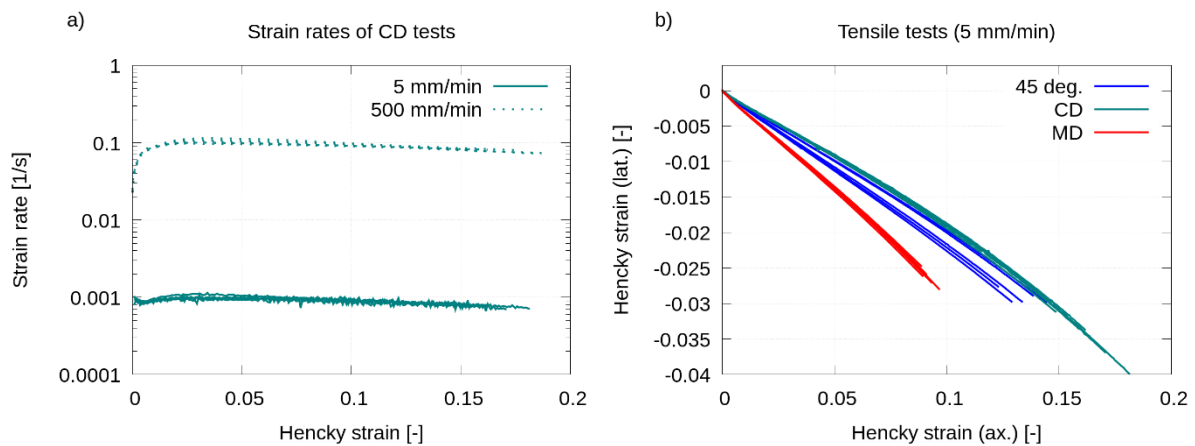


Fig.3: a) Calculated strain rates for both loading velocities and b) Hencky strain in axial and lateral direction

## 2.2 Punch tests

Punch tests were conducted to validate the parameters for **\*MAT\_PAPER** obtained from tensile tests. The experimental setup with an exemplary specimen is shown in Fig. 4. The specimen was clamped between two aluminum plates of 10 mm thickness. Both have a hole of 70 mm diameter in the middle. The clamping was done by first fixing the specimen on the top of the lower plate with tape. The lower plate was sand blasted on the specimen's side. A rubber ring (NBR, Nitrile Butadiene Rubber) was placed between the specimen and the upper plate to ensure fixation of the specimen during testing. The ring was 5 mm thick and had an inner diameter of 72 mm. The plates were fixed with screws to apply clamping pressure on the ring and the specimen. To calibrate the FE model, the deformation of the ring after fixation of the upper plate was determined to ~2 mm.

A punch with a diameter of 10 mm at a testing velocity of 1 mm/s and a 2 kN load cell were used. GOM ARAMIS 12M system was used to capture the displacement and the strain field during the experiments. The specimens were not preconditioned as the clamping and testing is more time consuming than the tensile tests. All tests were carried out under laboratory conditions. A total number of three specimens were tested.

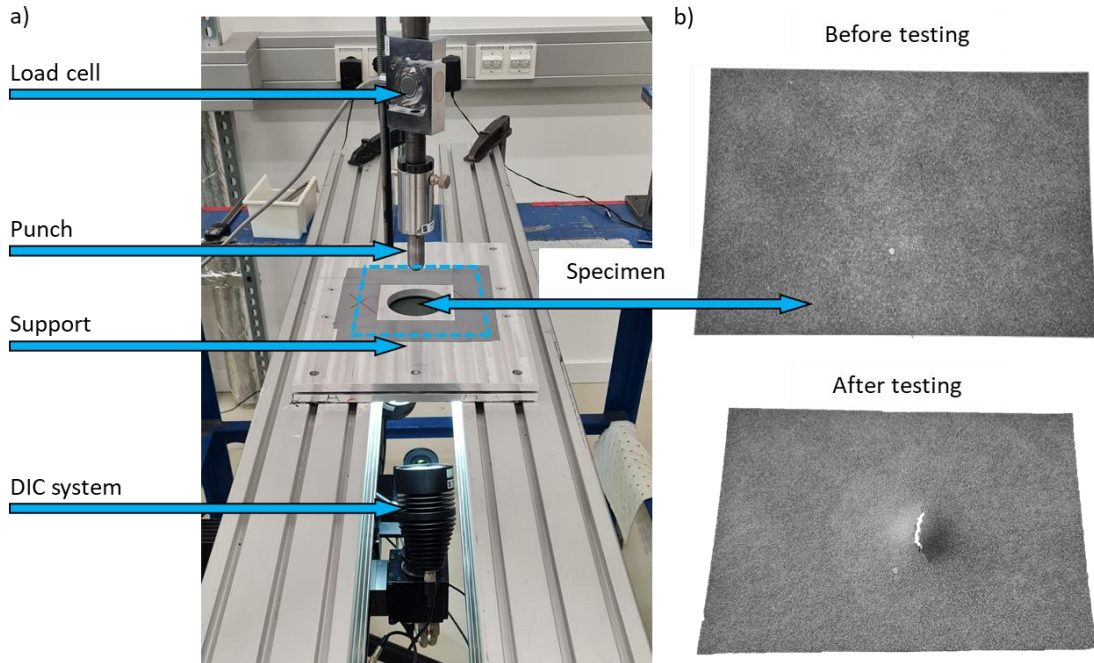


Fig.4: a) Experimental setup of the punch tests with punch, 3D camera system and the clamped specimen b) specimen before and after testing

The DIC data was used to obtain the displacement from the tests. Therefore, the maximum displacement at the bottom of the specimen was determined and the corresponding force-displacement curves are shown in Fig. 5.

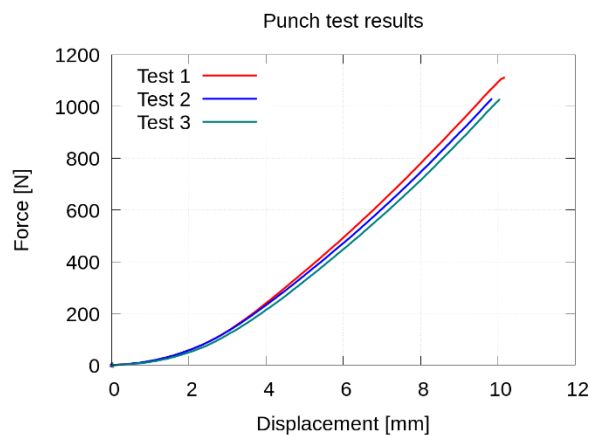


Fig.5: Experimentally obtained force-displacement curves from punch tests

DIC was also used to measure the deflection of the lower plate. The displacement around the edge of the circular hole was determined as an average  $\sim 0.15$  mm, which was assumed to be negligible in comparison to the displacement at the bottom of the specimen.

### 3 Numerical investigation

Both implicit simulations with the UMAT and explicit simulations with **\*MAT\_PAPER** were calibrated to represent the experimentally obtained stress-strain curves from tensile tests. For accurately capturing the experimental punch test setup the clamping was modeled. Therefore, a simplified characterization of the NBR ring was carried out. To investigate the influence of the model discretization a convergence study for different mesh sizes was conducted and a parameter study of different coefficients of friction (COF) was carried out.

### 3.1 Model calibration

As **\*MAT\_PAPER** captures no strain rate effects, the following parameter fitting was carried out for the lower strain rate of  $\sim 0.001$  /s. The results from the in-plane tensile tests (Fig 2 a) and 3 b)) were used to calibrate the corresponding parameters used by **\*MAT\_PAPER** to represent the material behavior of Dynal®. The elastic stiffness in MD and CD was determined by fitting the initial part of the stress strain curves, see Fig. 6 a). The same procedure was used to determine the elastic Poisson ratios.

The in-plane yield and hardening parameters S01-S03, A01-A03, B01-B03 and C01-C03 as well as G12 and the plastic Poisson ratios PRP1 and PRP2 were determined via uniaxial simulations in MD, CD and 45°. As no in-plane compression tests were conducted, the corresponding in-plane hardening parameters were set equal to those used for tension. However, the plastic Poisson ratios under compression were set to 0.001 to obtain comparability to the simplified UMAT. The elastic out-of-plane stiffness E3 was estimated from literature [6], whereby plastic behavior was neglected to simplify the parametrization. As no data was available for the out-of-plane shear behavior, the elastic constants G23 and G13 were arbitrarily set to 200 MPa and plastic effects were also neglected.

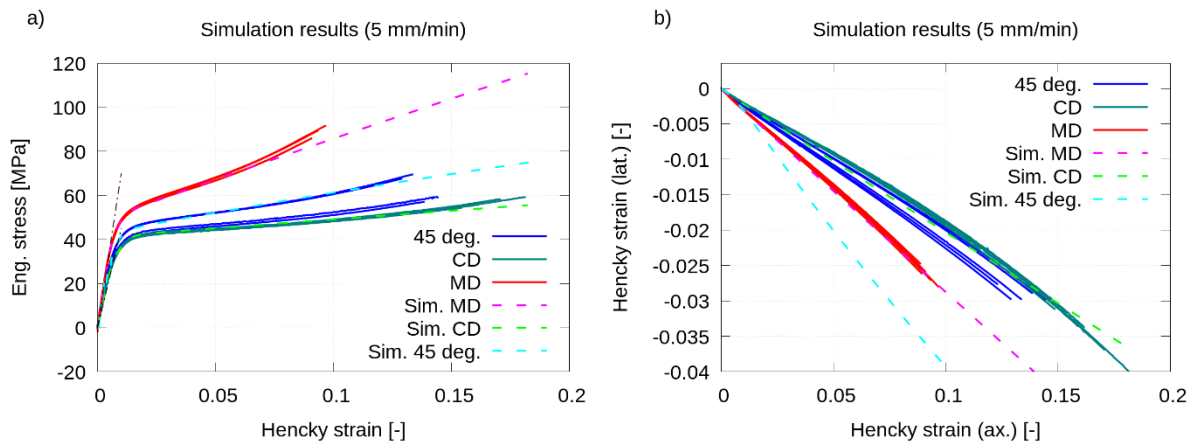


Fig.6: Comparison of experimental and numerical results after calibration of **\*MAT\_PAPER** a) stress-strain and b) lateral strain vs. axial strain

The material parameters used within this study are given in Tab. 1. The multiaxial behavior is also influenced by the parameter TWOK, which governs the round-off of the different yield planes [8]. No multiaxial data was used to calibrate the model so TWOK=2 was set to achieve comparability with the UMAT formulation. The resulting uniaxial behavior of the calibrated **\*MAT\_PAPER** model is shown in Fig. 6 a) and b). The lateral strain behavior of the 45° off-axis was not captured well with the presented set of material parameters, which were determined solely with respect to the stress strain behavior under uniaxial tension. A better result may be obtained by adjusting the in-plane shear hardening to the stress and lateral strain simultaneously.

<b>RO</b>	<b>E1</b>	<b>E2</b>	<b>E3</b>	<b>PR21</b>	<b>PR32</b>	<b>PR31</b>		
1.2E-6	7.08	4.97	3	0.227	1E-4	1E-4		
<b>G12</b>	<b>G23</b>	<b>G13</b>	<b>E3C</b>	<b>CC</b>	<b>TWOK</b>	<b>ROT</b>		
2.529	0.2	0.2	3	1	2	0		
<b>S01</b>	<b>A01</b>	<b>B01</b>	<b>C01</b>	<b>S02</b>	<b>A02</b>	<b>B02</b>	<b>C02</b>	
0.033	0.016	350	0.4	0.03	0.011	230	0.09	
<b>S03</b>	<b>A03</b>	<b>B03</b>	<b>C03</b>	<b>S04</b>	<b>A04</b>	<b>B04</b>	<b>C04</b>	
0.02	0.016	340	0.18	0.035	0.016	350	0.42	
<b>S05</b>	<b>A05</b>	<b>B05</b>	<b>C05</b>	<b>PRP1</b>	<b>PRP2</b>	<b>PRP4</b>	<b>PRP5</b>	
0.03	0.011	230	0.085	0.28	0.2	0.001	0.001	
<b>ASIG</b>	<b>BSIG</b>	<b>CSIG</b>	<b>TAU0</b>	<b>ATAU</b>	<b>BTAU</b>			
(100000)	(0.05)	(-18)	100000	0.1	1			

Table 1: Material parameters used for **\*MAT\_PAPER** (values in brackets are not necessary for shell elements but were provided within the material card)

The UMAT was calibrated to represent the in-plane stress-strain behavior. A comparison to **\*MAT\_PAPER** is given in Fig. 7.

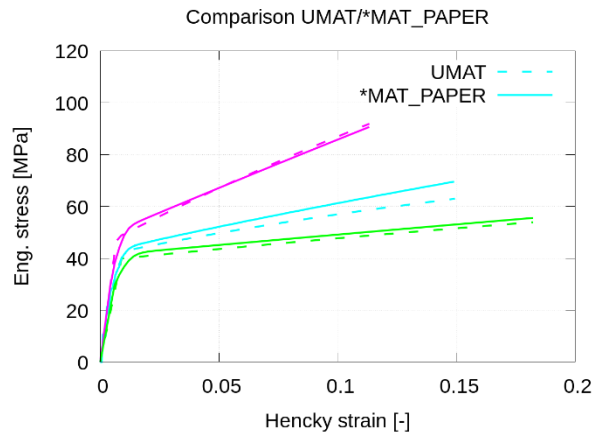


Fig.7: Comparison of the calibrated **\*MAT\_PAPER** and UMAT stress-strain responses

### 3.2 Model validation

To represent the boundary conditions of the punch test, e.g. the clamping force, the ring is included into the simulation. For a simplified characterization of the ring, compression tests were performed. Therefore, the ring was clamped between two plates and compressed 2 mm while force and displacement were measured. To neglect viscous effects, the displacement at peak load was held constant to obtain a relaxed stress state. **\*MAT\_MOONEY\_RIVLIN** with  $B=0$  (i.e. Neo-Hooke) material model was used and the material constants were approximated in a reverse engineering process until the relaxed clamping force value at 2 mm compression was reached. Fig. 8 shows a comparison of the measured and the simulated force displacement behavior of the ring after adjusting the material constants to  $\nu=0.495$  and  $A=0.767E-3$ .

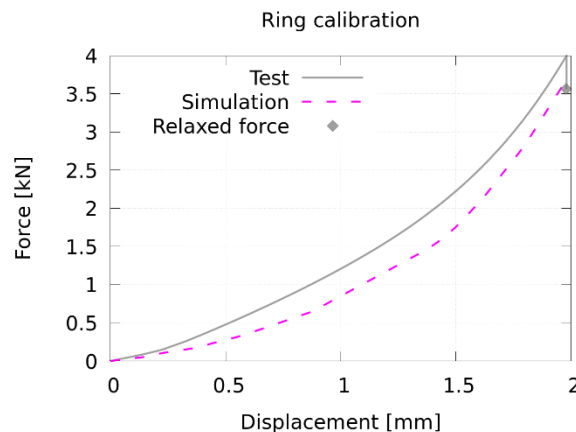


Fig.8: Comparison of ring compression tests with simulation results using **\*MAT\_MOONEY\_RIVLIN**

By taking advantage of the symmetry only  $\frac{1}{4}$  of the actual test setup is represented in FEM calculations. The FEM model is shown in Fig. 9.

Two steps of prescribed displacement are performed in the simulation. First, the clamping is performed by moving the upper plate 2 mm towards the specimen. After that, the punch is pressed into the sample. The upper and lower plate as well as the punch are modelled as rigid bodies. **MORTAR** contacts between the individual parts were used.

Different combinations of mesh size and different COF were used to determine the final simulation setup used to represent the experiments. Therefore, implicit simulations using the UMAT were performed to exclusively investigate the influences on the force-displacement results by neglecting dynamic effects.

The characteristic element lengths for the different mesh sizes and corresponding results are shown in Fig. 9 and Fig. 10 a), respectively. Only insignificant influences were found i.e. a mesh size of 1.25 mm was assumed to be sufficient to represent the deformation of the specimen at a moderate calculation time.

A comparable study was performed for COF. The COF were set equal for all contacts present within the model to reduce the number of necessary simulations. A noteworthy influence on the force-displacement behavior was found (see Fig. 10 b)) so it was necessary to approximate COF for the different contact partners from literature.

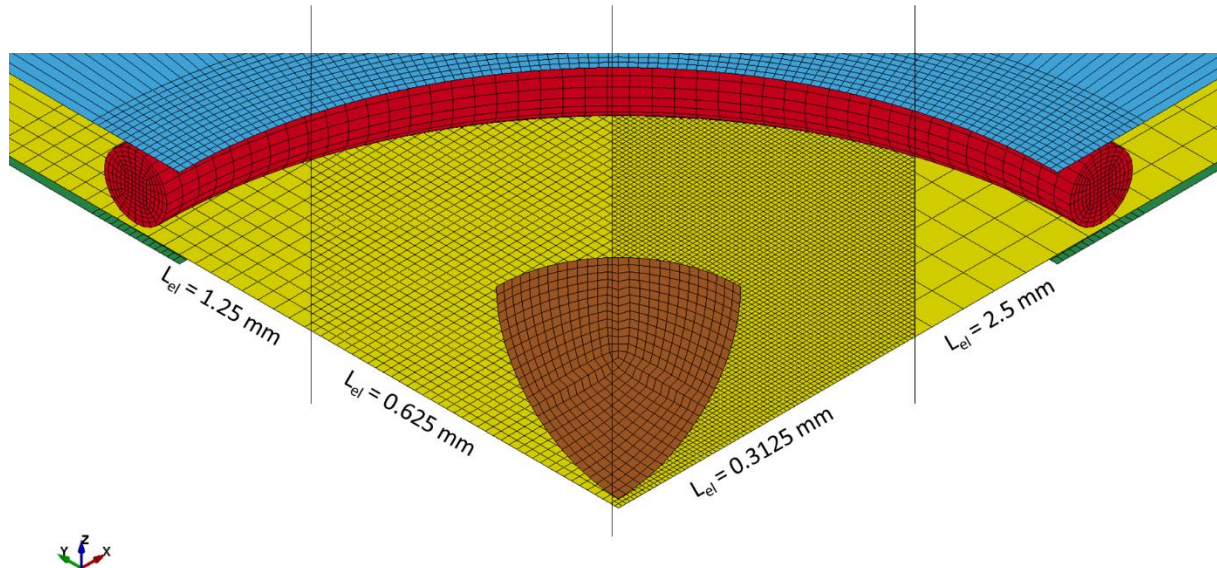


Fig.9: Simulation model of the punch test setup using symmetric boundary conditions. Different tested mesh sizes (mesh 1:  $L_{el} = 2.5$  mm, mesh 2:  $L_{el} = 1.25$  mm, mesh 3:  $L_{el} = 0.625$  mm, mesh 4:  $L_{el} = 0.3125$  mm) to determine the final model are shown

From [11] a COF of  $\sim 0.3$  for steel vs. paper is deduced which was used in this study for the contact between vulcanized fiber and aluminum. However, the transferability might be complained about. From [12] a COF of 0.7 was approximated for NBR and aluminum. As no data was available, the same COF was used for NBR and vulcanized fiber.

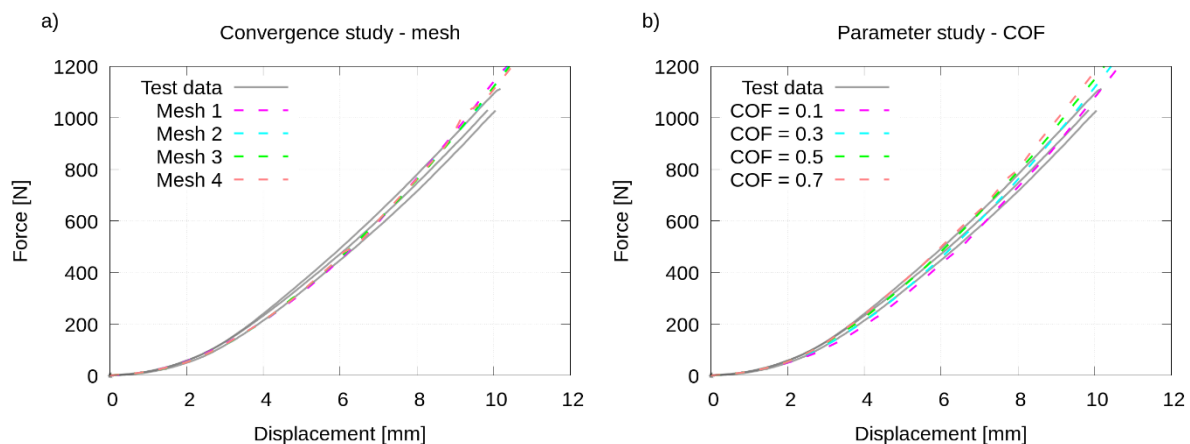


Fig.10: Simulation results of punch test for different a) mesh densities, b) coefficients of friction

After determining the final setup of the simulation model, implicit and explicit calculations of the punch tests were performed. For the implicit calculation, no difference was found when `*CONTROL_IMPLICIT_DYNAMICS` was included. The simulation results and the experimental results are shown in Fig. 11. The explicit simulation was performed with both `*MAT_PAPER` and the UMAT.

From Fig. 11 it is clear that the explicit calculation introduces artificial dynamic effects which lead to a significant change of simulation results as the test speed of 1 mm/s does not allow to represent the actual testing time in explicit simulations. Different calculation times as well as mass scaling and damping were applied to reduce the difference between explicit and implicit calculations. However, no significant improvement was achieved.

The good agreement of the implicit simulation results with the experimental data indicates that the approach used within **\*MAT\_PAPER** is able to represent the constitutive behavior of Dynal<sup>®</sup>. Furthermore, it must be pointed out that only uniaxial in-plane experiments were used to determine the necessary material parameters, but multiaxial loading is present during punch tests.

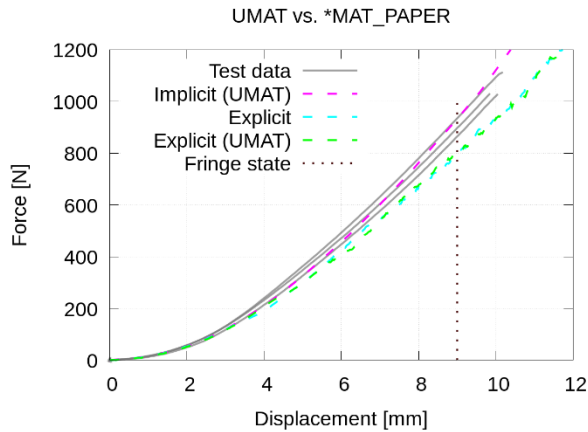


Fig. 11: Comparison of experimental results and implicit and explicit simulation results of the final setup with the UMAT and **\*MAT\_PAPER**

The experimental and numerical strain fields for a selected representative point were compared. Therefore, the Hencky strain of the representative point belonging to the simulation results from Fig. 11 and DIC measurements is shown in Fig. 12 in MD and CD. The depicted implicit simulation in Fig. 12 was carried out with the UMAT, whereas the explicit simulation was carried out with **\*MAT\_PAPER**. The results show good agreement of the calculations with the DIC data from the experiments. Similar results were obtained in [13] for paper using a sophisticated approach for the in-plane constitutive behavior.

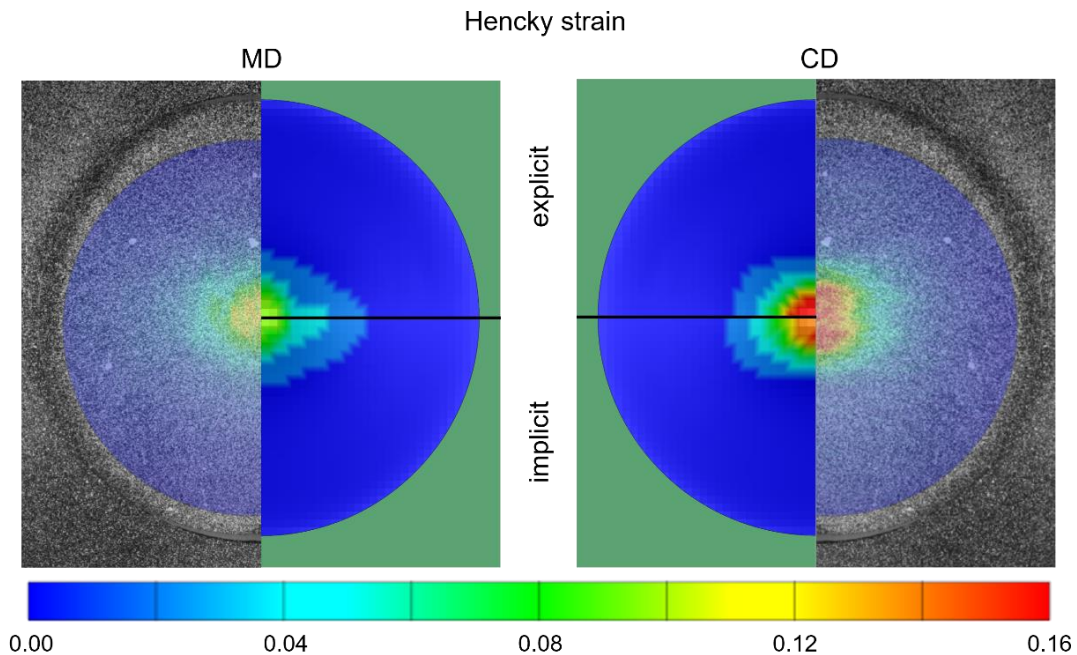


Fig. 12: Comparison of strain fields in MD and CD for explicit calculation using **\*MAT\_PAPER** and implicit calculation using UMAT with DIC results

## 4 Summary

The uniaxial material behavior of vulcanized fiber was tested experimentally by low strain rate tensile tests to obtain in-plane material parameters for **\*MAT\_PAPER**. For the comparability between **\*MAT\_PAPER** and an UMAT the material parameters for each were calibrated until a good agreement was found with the experimental data from tensile tests.

To validate the material parameters for multiaxial loading situations, punch tests were performed. Implicit simulations for studies regarding the discretization of the model and coefficients of friction (COF) were carried out with an UMAT. No significant influence was found for the convergence study with different mesh sizes. The parameter study showed an impact of COF on the force-displacement behavior. The final parameters were set and simulations with the UMAT, both implicit and explicit, were performed and compared. A final explicit simulation of the punch test with **\*MAT\_PAPER** was conducted. Implicit and explicit simulations show comparable results until artificial dynamic effects due to time scaling in explicit simulation occur. Overall, the final explicit simulation with **\*MAT\_PAPER** is in good agreement with experimental data and the capability of **\*MAT\_PAPER** to represent vulcanized fiber is showed.

## Acknowledgements

The authors would like to thank the Hessian Ministry for the financial support within the framework of the research funding "Promotion of Electromobility in Hesse".

## 5 Literature

- [1] Taylor T.: "Improvement in the treatment of paper and paper-pulp", U.S. Patent 114,880, 1871
- [2] Domininghaus H.: "Die Kunststoffe und ihre Eigenschaften", Springer, 1998
- [3] Brown W.: "Vulcanized Fibre – An Old Material With A New Relevancy", NVF Company, 1999
- [4] Scholz R., Engels J., Hartmaier A., Künne B., Walther F.: "Direction-dependent mechanical characterization of cellulose-based composite vulcanized fiber", 58, Materials Testing, 2016, 813-817
- [5] Meyer K.: "Technologie des Maschinentechnikers", Verlag von Julius Springer, 1920
- [6] Fiedler Bremer C., Scholz R., Myslicki S., Starke P., Boller C., Walther F., Krause M.: "NDT-Based Characterization of Timber and Vulcanized Fiber for Civil Infrastructure", International Symposium Non-Destructive Testing in Civil Engineering (NDTCE 2015-11), 2015
- [7] Karlsson, J., Schill, M., Tryding, J.: "**\*MAT\_PAPER** and **\*MAT\_COHESIVE\_PAPER**: Two New Models for Paperboard Materials", 14<sup>th</sup> International LS-DYNA Users Conference, 2016
- [8] Xia, Q. S., Boyce, M. C., & Parks, D. M.: "A constitutive model for the anisotropic elastic-plastic deformation of paper and paperboard". International journal of solids and structures, 39(15), 2002, 4053-4071
- [9] Pfeiffer, M., Kolling, S.: "A non-associative orthotropic plasticity model for paperboard under in-plane loading", International Journal of Solids and Structures, 166, 2019, 112-123
- [10] Nygård, M.: "Experimental techniques for characterization of elastic-plastic material properties in paperboard", Nordic Pulp and Paper Research Journal, 23, 2008, 432-437
- [11] Huttel, D.: "Wirkmedienbasiertes Umformen von Papier", Dissertation, in: Berichte aus Produktion und Umformtechnik, 97, Aachen, Shaker, 2015
- [12] Gao, H., Guo, Y., Bao, G., Reynaerts, D.: "Influence of vibrated area and normal force on friction reduction ratio between NBR/aluminum couple", Tribology International, 82, 2015, 95-100
- [13] Li, Y., Stapleton, S. E., Reese, S., Simon, J.-W.: "Anisotropic elastic-plastic deformation of paper: In-plane model", International Journal of Solids and Structures, 100-101, 2016, 286-296